national accelerator laboratory

NAL-Conf-73/31-EXP
7200.037

UCLA-1075

(Submitted to the International Conf. on New Results from Experiments on High Energy Particle Collisions, Vanderbilt University, March 26-28, 1973)

# pp INTERACTIONS AT 303 GeV/c: INCLUSIVE STUDIES OF $\gamma$, $K^o_S$, $\Lambda^o$, $\pi^{\pm}$, AND PROTON PRODUCTION

F. T. Dao, D. Gordon, J. Lach, E. Malamud, and J. Schivell
National Accelerator Laboratory
Batavia, Illinois 60510

and

T. Meyer, R. Poster, P. E. Schlein, and W. E. Slater
University of California at Los Angeles
Los Angeles, California 90024

May 1973

Operated by Universities Research Association Inc. Under Contract with the United States Atomic Energy Commission

NAL-Conf-73/31-EXP
7200.037

pp INTERACTIONS AT 303 GeV/c: INCLUSIVE STUDIES OF $\gamma$, $K_S^0$, $\Lambda^0$, $\pi^{\pm}$ AND PROTON PRODUCTION

F. T. Dao, D. Gordon, J. Lach, E. Malamud, J. Schivell
National Accelerator Laboratory, Batavia, Illinois 60510

T. Meyer, R. Poster, P. E. Schlein, W. E. Slater*
University of California, Los Angeles, California 90024

Talk Presented by F. T. Dao and R. Poster at the International Conference on New Results from Experiments on High Energy Particle Collisions, Vanderbilt University, March 26-28, 1973

ABSTRACT

In an exposure of the 30 inch hydrogen bubble chamber to a 303 GeV/c proton beam, we have measured both $V^0$ events and all tracks with momentum less than 1.4 GeV/c. From these measurements, the properties and cross sections of the inclusive pp $\to \gamma X$, $K_S^0 X$, and $\Lambda^0 X$ reactions are studied. In addition, single particle invariant cross sections for pion and proton production are presented and the scaling behavior of these reactions is discussed.

*Supported by the U.S. National Science Foundation under Grant GP 33565

NAL-Conf-73/31-EXP
7200.037

# INCLUSIVE STUDIES OF $\gamma$, $K_S^0$, AND $\Lambda^0$ PRODUCTION

In the first part we report on the study of $V^0$ events from an exposure of 205 GeV/c and 303 GeV/c protons in the 30-inch hydrogen bubble chamber at the National Accelerator Laboratory. Preliminary results at 205 GeV/c have been published.[1] These $V^0$ events were measured and processed through TVGP and SQUAW and fitted to the following hypotheses: $K_S^0 \to \pi^+\pi^-$, $\Lambda^0 \to p\pi^-$, $\bar{\Lambda}^0 \to \pi^+\bar{p}$, and $\gamma(p) \to e^+e^-(p)$.

The data for $K_S^0$, $\Lambda^0$, and $\bar{\Lambda}^0$ were restricted to the backward hemisphere in the pp center of mass as the detection efficiency in the forward direction was extremely low. Table I summarizes the $V^0$ sample at 303 GeV/c. The average weighting factors[2] are: 71.9 for $\gamma$, 3.44 for $K_S^0$, 4.25 for $\Lambda^0$, and 4.69 for $\bar{\Lambda}^0$. The final sample was further corrected by a scanning efficiency of 0.93. The inclusive cross sections measured are: $\sigma(\gamma) = 253 \pm 24$ mb, $\sigma(K_S^0) = 9.8 \pm 1.3$ mb, $\sigma(\Lambda^0) = 4.2 \pm 1.0$ mb, and $\sigma(\bar{\Lambda}^0) = 0.4^{+1.0}_{-0.3}$ mb. Assuming that all $\gamma$'s come from $\pi^0 \to 2\gamma$, we get $\sigma(\pi^0) = (127 \pm 12)$mb.

The dependencies of these cross sections on the incident laboratory momentum[1,3,4] are shown in Figs. 1(a), (b), and (c). Note that $\sigma(\Lambda^0)$ has increased threefold from 28 GeV/c to 303 GeV/c and remains much larger than $\sigma(\bar{\Lambda}^0)$ at 303 GeV/c. The $K_S^0$ cross section has increased more than eight times from 28 GeV/c to 303 GeV/c. However, the rapid rise in $\sigma(K_S^0)$ may level off at energies beyond 303 GeV/c as indicated by the ISR data.[5] The $\pi^0$ cross section in Fig. 1(c) is consistent with a logarithmic growth with incident momentum and is equal to $\sigma(n_-)$ or $\sigma(\pi^-)$ if we assume all negatively charged particles to be $\pi^-$'s. This is in accord with multiperipheral models that predict $\langle n_{\pi^0}\rangle = \langle n_{\pi^-}\rangle = \langle n_{\pi^+}\rangle$[6] where $\langle n_x\rangle$ is the average number of particles of type x produced per inelastic pp collision.

The topological cross sections, $\langle n_{\pi^0}\rangle$ and $\langle n_{K_S^0}\rangle$ for inclusive $\pi^0$ and $K_S^0$ production at 303 GeV/c are listed in Table II.

In Fig. 2(a) and (b) $\langle n_{\pi^0}\rangle$ and $\langle n_{K_S^0}\rangle$ are plotted as a function of charged multiplicity, $n_c$. Two possible dependencies are shown: $\langle n_{K_S^0}\rangle = 0.31$ assumes $K_S^0$ production is independent of topology; $\langle n_{K_S^0}\rangle = 0.09\, n_-$ is based on $\sigma_{K_S^0}/\sigma_{\pi^-}$ being independent of topology. In particular, $\langle n_{\pi^0}\rangle$ tends to rise linearly with $n_c \leq 18$. The latter linear dependence is very different from the low energy pp data.[7]

The broken straight line in Fig. 2(b) is given by $\langle n_{\pi^\circ} \rangle = n_-$. If we assume all the negative particles to be pions, the data imply that the neutral and charged pions are strongly correlated. This behavior rules out models in which pions are independently emitted but is in accord with fragmentation models and multi-peripheral models in which $\rho$ and $\omega$ type meson clusters are emitted.[8]

A systematic study on the energy dependence of the correlation in $n_{\pi^\circ}$ versus $n_-$ has been made recently.[9] The data from pp,[7, 10, 11] $\pi^{\pm}p$,[12] and $\pi^- n$[13] collisions in laboratory beam momentum ranging from 12 GeV/c to 1500 GeV/c were fitted to the linear form,

$$\langle n_{\pi^o} \rangle = \alpha n_- + \beta$$

where $\alpha$ and $\beta$ are energy dependent parameters. The parameter $\alpha$ would indicate the strength of the neutral and charged pion correlation. Figure 3 shows the result of such linear fits and Fig. 4 shows $\alpha$ as a function of E, which is the available energy in the cm system, that is, the total energy ($\sqrt{s}$) minus the number of baryon masses in the initial state. Present data indicate (1) $\alpha \simeq 0$ at low energies and approaches 1 at very high energies and (2) the strength of correlation is relatively independent of the initial state particles. The solid curve is a prediction based on Thomas' critical fluid model.[14] This model also predicts at high energy

$$\alpha_K \simeq (\sigma_K/\sigma_\pi) \cdot \alpha$$

where $\alpha_K$ is the strength of correlation between kaons and pions. The data given in Fig. 2(a) may show such a trend.

The invariant single particle distributions for $\gamma$'s in Feynman variable $x$ and transverse momentum $p_T^2$ are shown in Figs. 5(a) and (b). Note that scaling holds at 205 and 303 GeV/c. A prominent forward peak is noted at both energies for $p_T^2 \leq 0.02$ $(\text{GeV/c})^2$. In Fig. 6(a) and (b) $\langle p_T \rangle$ is plotted as a function of x. The weighting introduced by the gamma energy $E_\gamma$ does not change appreciably the presence of a strong correlation for small values of x, indicating that the invariant single particle distribution cannot be factorized into a product involving x and $P_T^2$.

In Figs. 7(a) and (b), we show the invariant single particle distribution for the inclusive $K_S^o$ and $\Lambda^o$ reactions. Results at 303 GeV/c combined with the 205 GeV/c data give evidence that the inclusive $K_S^o$ and $\Lambda^o$ reactions have reached their scaling limits from below, with $\Lambda^o$ approaching the limit at a much faster rate than $K_S^o$.

Figures 8(a) and (b) show $d\sigma/dy$ versus the rapidity variable $y$ for the $K^{o}_{s}$ and $\gamma$ reactions at 303 GeV/c. There is evidence for a plateau with widths of two units in $y$ for the $K^{o}_{s}$ and low multiplicity $\gamma$ events; $d\sigma/dy$ semms to peak at $y = 0$ for high multiplicity $\gamma$ events. The average longitudinal momentum in the center of mass $p_L$ = 2.90 ± 0.56, 1.11 ± 0.17, and 0.88 ± 0.12 GeV/c for $\Lambda^{o}$, $K^{o}_{s}$, and $\pi^{o}$, respectively.[15] Thus, neutral pions and kaons are produced more frequently in the central region than $\Lambda^{o}$'s.

## SCALING IN SINGLE PARTICLE $\pi^{\pm}$ AND PROTON DISTRIBUTIONS

In this second section we present results of single particle $\pi^{\pm}$ and proton invariant cross section distributions. These distributions are compared with existing data at higher CM energy from the CERN-ISR and at lower CM energy from the CERN-PS and the BNL-AGS.

As described in our earlier paper on $\Delta^{++}(1236)$ production,[17] particles which travel backward in the pp center-of-mass have comparatively low momenta in the laboratory and can be measured with conventional film measuring machines and analysis techniques. Such measurements have been performed on all tracks with laboratory momenta $P_{lab} \leq 1.4$ GeV/c. Since protons with this momentum have 1.4 x minimum ionization, pions and protons are distinguished with good reliability by their ionization. From the number of observed events involving $K^{o}_{S}$ emission as well as direct ionization information, we estimate that the amount of $K^{\pm}$ contamination in the $\pi$-proton sample is ~2-3%, which we ignore for the purposes of the present paper.

Of the 1750 events in the fiducial volume used for the present investigation, 806 events were found which have a single proton with $P_{lab} \leq 1.4$ GeV/c. To illustrate the kinematically accepted region and the overall qualitative properties of the data, the CM distribution of these protons in the variables $x = 2P_{\parallel}/\sqrt{s}$ and the transverse momentum $P_t^2$ is shown in Fig. 9(a). The cutoff seen on the right-hand side of the distribution is due to the selection of $P_{lab} \leq 1.4$ GeV/c.

Similar distributions for all $\pi^{+}$ and $\pi^{-}$ tracks are shown in Figs.9(b,c), respectively. The kinematic cutoff at low x corresponding to $P_{lab} = 1.4$ GeV/c is again seen in both plots. The remarkably different properties of pion and proton distributions are also apparent.

Before discussing the detailed properties of these distributions, we note that these data complement existing ISR data since first round inclusive ISR experiments have not explored the smallest angular region possible. This is illustrated by Fig. 10 (reproduced from the talk by J. C. Sens at the 1972 Oxford Conference). Lines for pions and protons with $P_{lab}$ = 1.4 GeV/c are superimposed. Our data explore the regions to the right of these curves and no further acceptance corrections are necessary.

In Figure 11, we demonstrate how the bubble chamber data complement the ISR data with a comparison between inclusive proton spectra of the CERN-Holland-Lancaster-Manchester [18] collaboration at $\sqrt{s}$ = 23.6, 30.8, and 44.6 GeV, respectively. The overall normalization agreement between the two sets of data is quite good as seen in the region of overlap. The bubble chamber data extends to lower values to $P_t$ than the ISR data. Although the ISR data points in themselves represent a rather impressive test of scaling over the $P_t$ and energy ranges they represent, they cutoff at $P_t$ = 0.5 GeV/c and thus our data at smaller $P_t$ values can only be compared with the lower energy data from BNL and CERN.[19]

Figures 12 (a-e) contain more detailed comparisons between the $P_t^2$-dependencies of $Ed^3\sigma/dp^3$ for protons at several different values of $\bar{x}$. The essential point of these plots is to illustrate the lack of $e^{-aP_t^2}$ behavior over the entire range of $P_t^2$. The straight lines are those fit by Albrow et al.[20] to their own data and are invariably much lower than the small $P_t^2$ data. With the exception of the lowest x value of 0.45, we observe that the 300 GeV data points are in good agreement with the 24 GeV/c data of Allaby et al. [19] for $P_t^2 \lesssim 0.5$ $(GeV/c)^2$. The relationship is more clearly displayed in Fig. 13 which compares the x-dependence of the invariant cross section $Ed^3\sigma/dp^3$ at a mean value of $P_t^2$ = 0.04 $(GeV/c)^2$ with the Allaby et al. data. While the low and high energy data are in reasonably good agreement, they suggest that scaling is approached from above (i.e. lower momenta data are larger).

In contrast to the proton data, our pion data more nearly covers the same x-$P_t$ range as existing ISR data and thus does not add anything essentially new to the scaling comparisons made between ISR and lower energy data. However, as illustrated in Fig. 10 , there is not a complete overlap; furthermore, most ISR data used for scaling comparisons are not at the lowest end of the energy range. Thus, our 300 GeV data ($\sqrt{s}$ = 23.9 GeV) are of some interest.

Figures 14 and 15 display the x-dependence of the invariant cross section for $\pi^+$ and $\pi^-$, respectively, at $P_t^2$ = 0.04 and

0.16 $(\mathrm{GeV}/c)^2$. In each case, scaling is seen to break down at small x for $P_t^2 = 0.04\ (\mathrm{GeV}/c)^2$. Figures 16a and 16b display the dependences on $P_t^2$ at $\bar{x} = 0.21$ for $\pi^+$ and $\pi^-$, respectively. Generally good agreement is observed, although there seem to be differences among the lowest energy data themselves.

## REFERENCES


1. G. Charlton et al., Phys. Rev. Letters 30, 574 (1973); G. Charlton et al., Phys. Rev. Letters 29, 1759 (1972).
2. Each event was weighted by a factor calculated from the potential decay length and neutral decay branching ratio. The minimum length for efficient detection was 4 cm for $\gamma$ and 2 cm for $K_S^0$, $\Lambda^0$, and $\bar{\Lambda}^0$. The pair conversion cross section for $\gamma$ was calculated by T. M. Knasel, DESY Reports Nos. 70/2 and 70/3.
3. B. Y. Oh and G. A. Smith, "Inclusive Study of $\Lambda^0$ and $\Sigma^\pm$ Hyperons Produced in Proton-Proton Collisions from 6.6 to 28 GeV/c", paper submitted at XVI International Conference on High Energy Physics, Batavia (1972).
4. G. Neuhofer et al., Phys. Letters 28B, 51 (1972); and Phys. Letters 37B, 438 (1971).
5. The ISR data points in Fig. 1(b) were computed on the assumption that neutral kaon emission is as frequent as charged kaon emission. Thus,

$$\sigma(K_S^0) \quad \left( \frac{R\left(\frac{K^+}{\pi^+}\right) + R\left(\frac{K^-}{\pi^-}\right) \quad R\left(\frac{\pi^-}{\pi^+}\right)}{1 + R\left(\frac{\pi^-}{\pi^+}\right)} \right) \quad \sigma(\pi^0)$$

   where the ratios were obtained from A. Bertin et al., Phys. Letters 41B, 201 (1972) and $\pi^0$ cross section from Ref. 9.
6. J. Honerkamp and K. H. Mütter, Nucl. Phys. B38, 565 (1972).
7. H. Bøggild et al., Nucl. Phys. B27, 285 (1971).
8. E. L. Berger, D. Horn, and G. H. Thomas, ANL/HEP Report 7240 (1972).
9. F. T. Dao and J. Whitmore, "Remarks on Particle Correlations in High Energy Collisions", NAL Report (1973).
10. J. H. Campbell et al., ANL Preprint (1973).

11. G. Neuhofer et al., Contribution to the XVI International Conference on High Energy Physics, Batavia (1972).
12. J. W. Elbert et al., Nucl. Phys. B19, 85 (1970); and private communication from A. Erwin.
13. JINR, Dubna Collaboration, "Analysis of the Experimental Data on Secondary Particle Multiplicity in $\pi^- p$, $\pi^- n$, and $\pi^- C$ Collisions at p = 40 GeV/c", contribution to the XVI International Conference on High Energy Physics, Batavia (1972).
14. G. H. Thomas, ANL Preprint ANL/HEP 7302 (1973).
15. H. J. Muck et al., Phys. Letters 39B, 303 (1972).
16. G. I. Kopylov, Nucl. Phys. B52, 126 (1973), derives

$$\langle p_L(\pi^0)\rangle = \langle p_L(\gamma)\rangle \times 2.$$

17. F. T. Dao et al., Phys. Rev. Lett. 30, 34 (1973).
18. J. C. Sens, private communication.
19. W. H. Sims et al., Nuc. Phys. B41, 317 (1972) and J. V. Allaby et al., contribution to the Fourth Int. Conference on High Energy Collisions, Oxford (1972).
20. M. J. Albrow et al., contributions to the 16th Int. Conference on High Energy Physics, Batavia (1972).

TABLE I

$pp \to V^0 X$ at 303 GeV/c

| $pp \to$ | $K_S^0$ | $\Lambda^0$ | $\overline{\Lambda}^0$ | $\gamma$ | $\pi^0 \to 2\gamma$ |
|---|---|---|---|---|---|
| No. of Events | 50 | 20 | 2(Unique) | 119 | -- |
| Average Weighting | 3.44 | 4.25 | 4.69 | 71.9 | -- |
| $\sigma$(mb) | 9.81 ± 1.36 | 4.22 ± 0.98 | $\gtrsim$0.42 | 253.4 ± 23.8 | 126.7 |
| $\langle n\rangle$/pp | 0.31 ± 0.04 | 0.13 ± 0.03 | $\gtrsim$0.01 | 7.90 ± 0.75 | 3.95 |
| $\langle p_T\rangle$ (GeV/c) | 0.47 ± 0.04 | 0.43 ± 0.04 | (0.40) | 0.17 ± 0.01 | ~0.38* |
| $\langle p_L\rangle$ | 1.11 ± 0.17 | 2.90 ± 0.56 | (0.31) | 0.44 ± 0.06 | 0.88* |

*See Ref. 16 for relations between $\pi^0$ and derived $\gamma$'s.

TABLE II

Cross Sections for $pp \rightarrow \pi^0 X$ and $K_S^0 X$
at 303 GeV/c

| n = Number of Charged Particles | $\sigma_n(pp \rightarrow \pi^0 X)$* in mb | $\langle n_{\pi^0} \rangle$ | $\sigma_n(pp \rightarrow K_S^0 X)$ in mb | $\langle n_{K_S^0} \rangle$ |
|---|---|---|---|---|
| 2 | 1.7 ± 1.2 | 1.0 ± 0.7 | 0.2 ± 0.2 | 0.1 ± 0.1 |
| 4 | 11.8 ± 3.1 | 2.4 ± 0.7 | 0.8 ± 0.4 | 0.2 ± 0.1 |
| 6 | 19.4 ± 4.1 | 3.4 ± 0.8 | 2.9 ± 0.7 | 0.5 ± 0.1 |
| 8 | 16.0 ± 3.7 | 3.0 ± 0.7 | 1.4 ± 0.5 | 0.3 ± 0.1 |
| 10 | 22.8 ± 4.4 | 4.8 ± 1.0 | 1.6 ± 0.5 | 0.4 ± 0.1 |
| 12 | 20.3 ± 4.1 | 4.8 ± 1.4 | 1.3 ± 0.4 | 0.3 ± 0.1 |
| 14 | 15.7 ± 2.5 | 7.2 ± 1.5 | 0.6 ± 0.2 | 0.3 ± 0.1 |
| 16 | 9.3 ± 2.8 | 6.7 ± 2.2 | 0.8 ± 0.4 | 0.6 ± 0.3 |
| 18 | 7.2 ± 2.5 | 8.3 ± 3.2 | --- | --- |
| 20 | 1.6 ± 1.1 | 3.3 ± 2.4 | 0.2 ± 0.2 | 0.3 ± 0.3 |
| 22 | --- | --- | --- | --- |
| 24 | --- | --- | --- | --- |
| 26 | 0.9 ± 0.9 | 17.0 ± 17.0 | --- | --- |
| TOTAL | 127.0 ± 12.0 | 3.94 ± 0.39 | 9.8 ± 1.3 | 0.31 ± 0.04 |

*Calculated from $\sigma_n(pp \rightarrow \pi^0 X) = \sigma_n(pp \rightarrow \gamma X)/2$ .

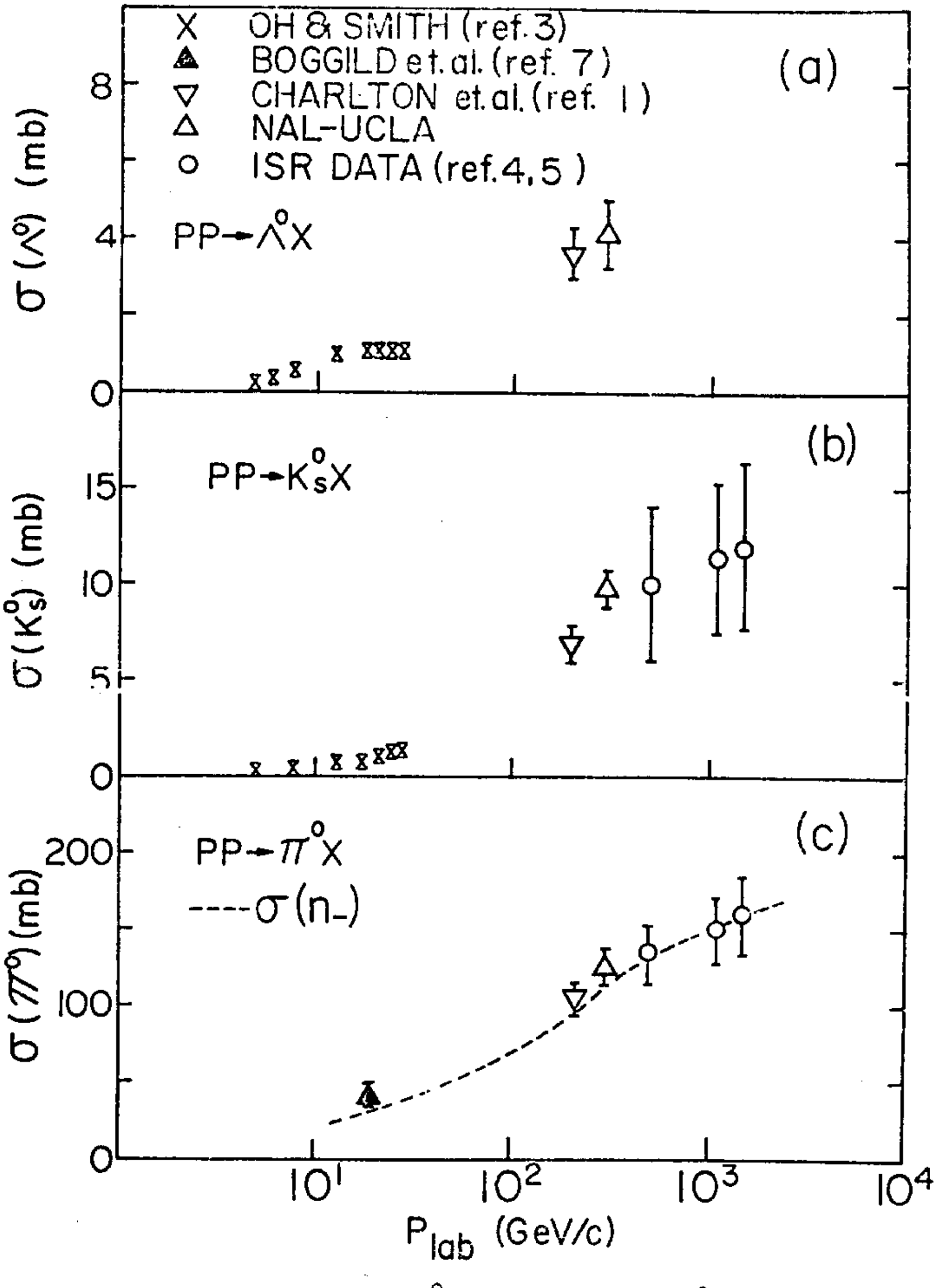


Fig. 1. (a) $\sigma(pp \to \Lambda^0 X)$, (b) $\sigma(pp \to K_S{}^0 X)$, and (c) $\sigma(pp \to \pi^0 X)$ versus incident laboratory momentum $P_{lab}$. The data points beyond 303GeV/c in (b) are as derived in Ref. 10.

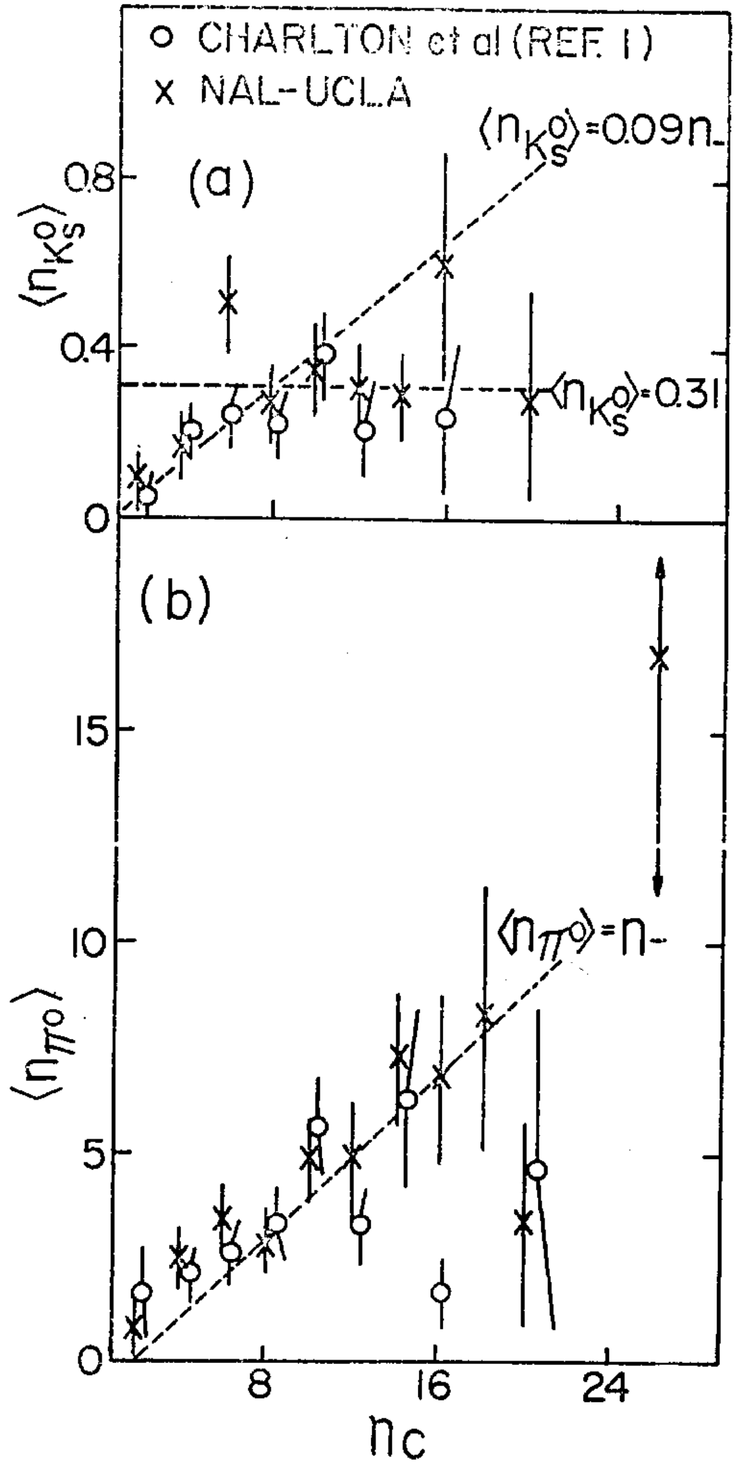


Fig. 2. (a) Average number of $K_S^o$ and (b) average number of $\pi^o$'s produced per inelastic pp collision versus charge multiplicity. The curves are described in the text.

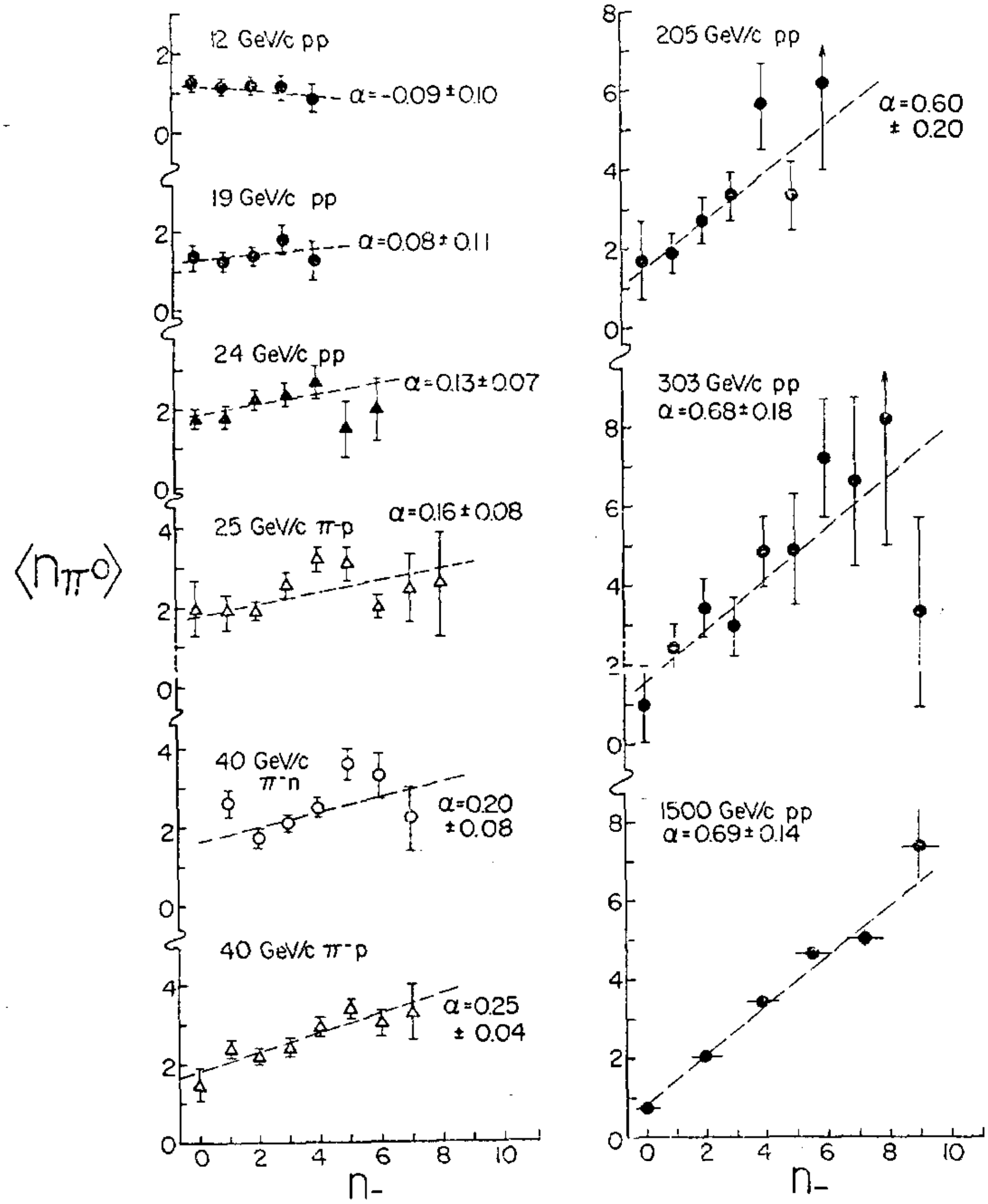


Fig. 3. $<n_{\pi}o>$ versus $n_-$ for pp, $\pi$p, and $\pi$n collisions. The $\alpha$'s are obtained from fitting $<n_{\pi}o> = \alpha n_- + \beta$ to the data.

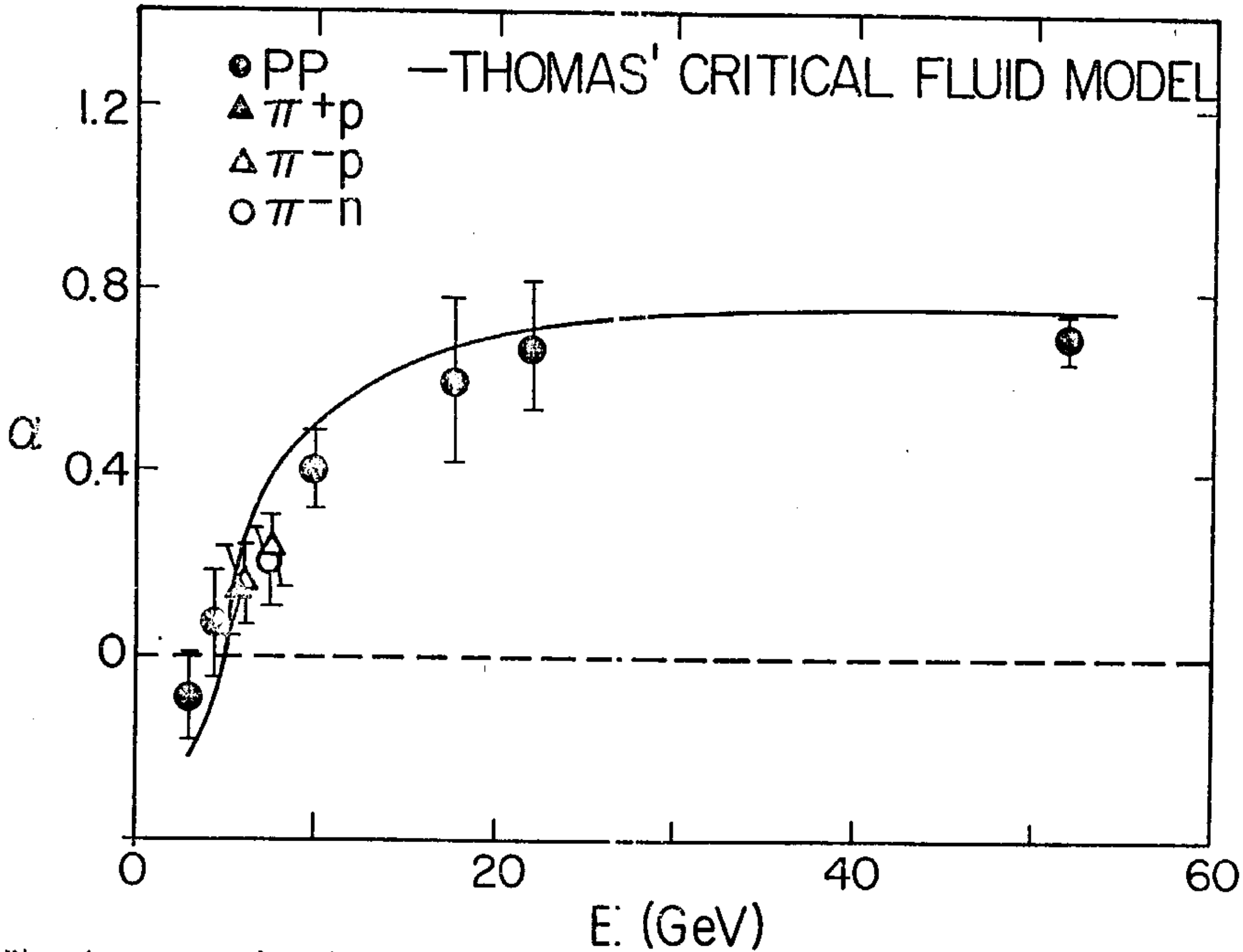


Fig. 4. $\alpha$ as a function of available energy E (see text for definition). The solid curve is a prediction of Thomas's critical fluid model (Ref. 14).

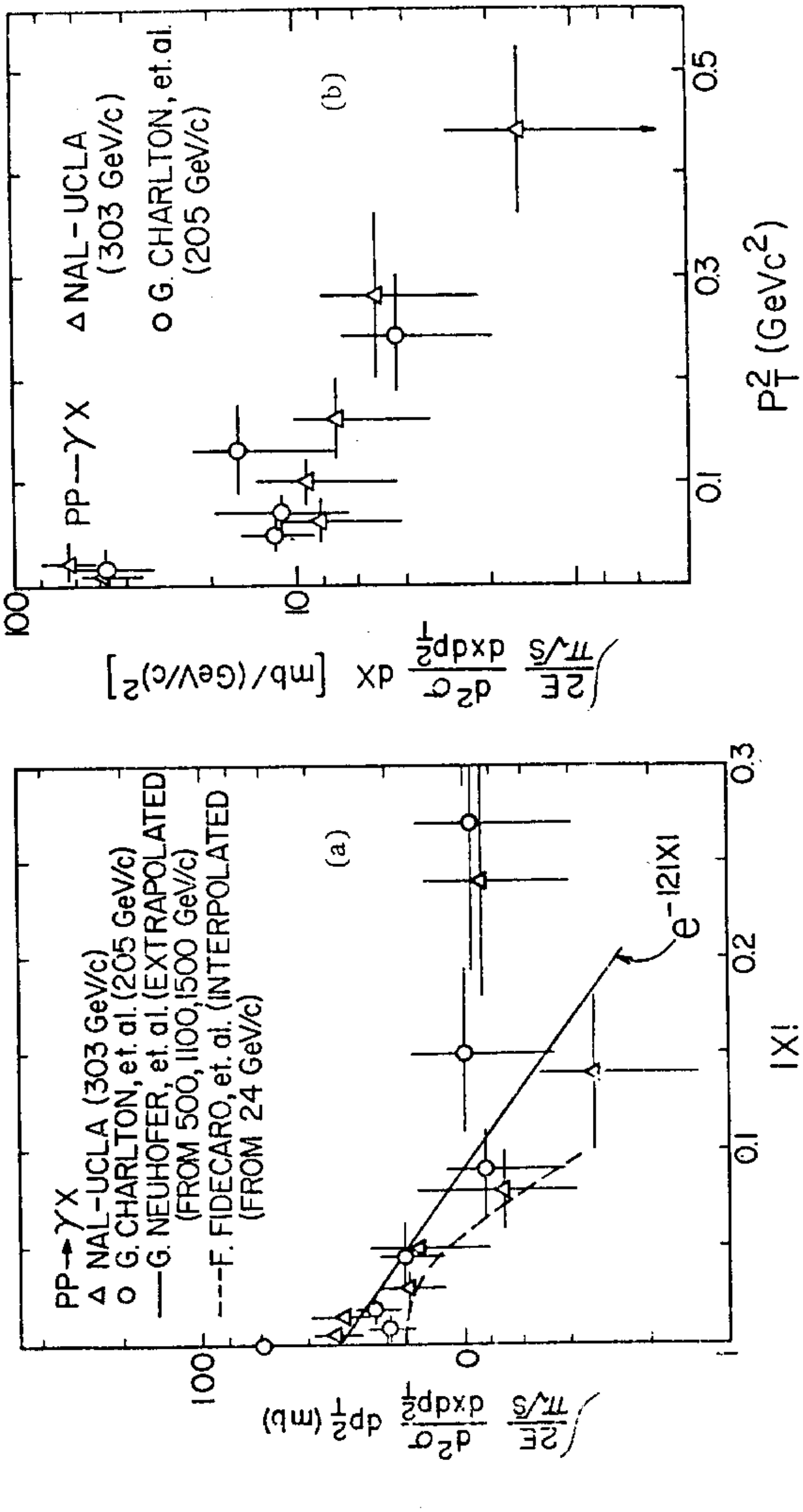


Fig. 5. (a) The invariant cross section integrated over $P_t^2$ versus x for pp → γX, and (b) the invariant cross section integrated over x versus $P_t^2$.

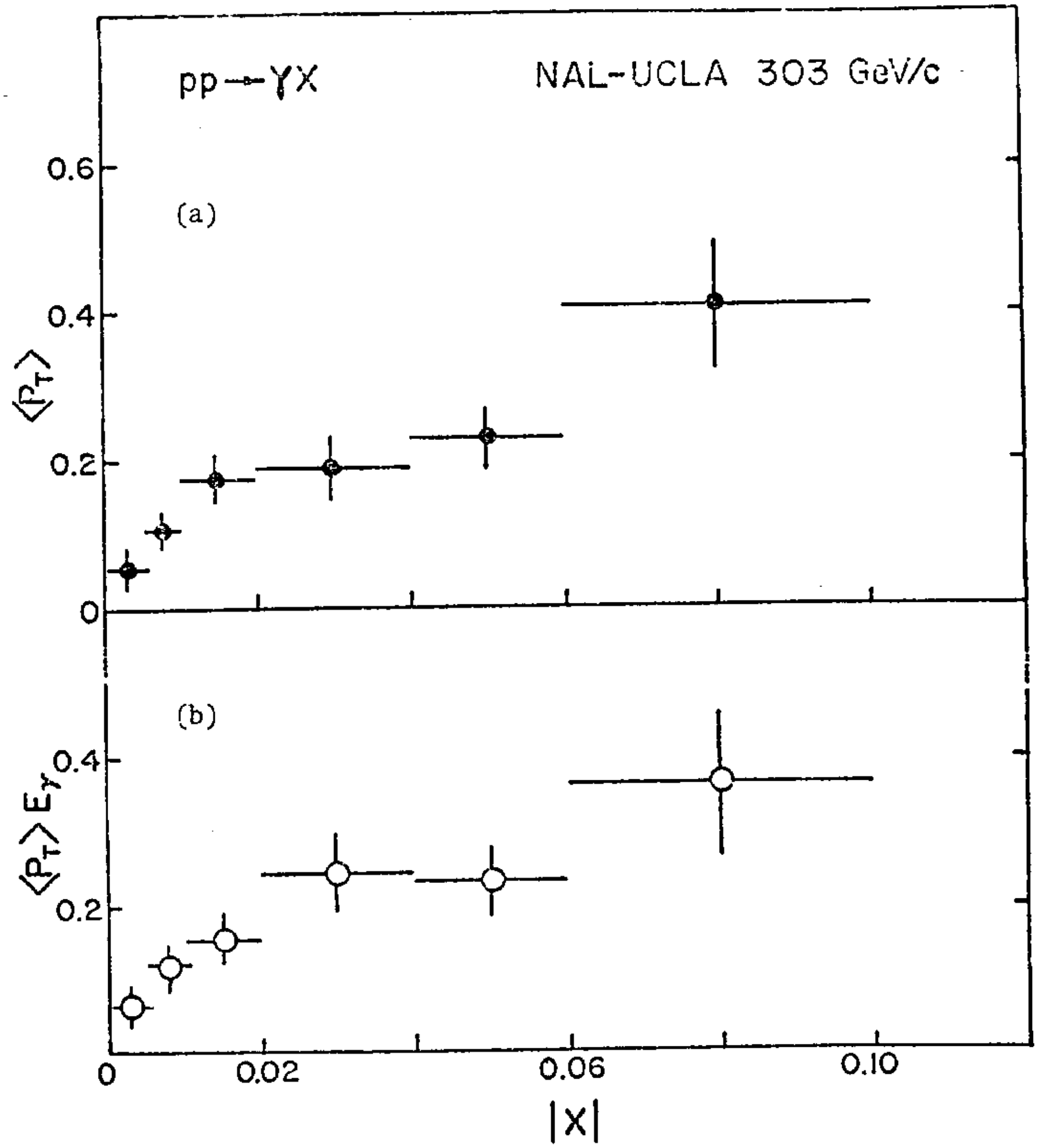


Fig. 6. (a) $<P_t>$ versus x and (b) $<P_t>E_\gamma$ versus x.

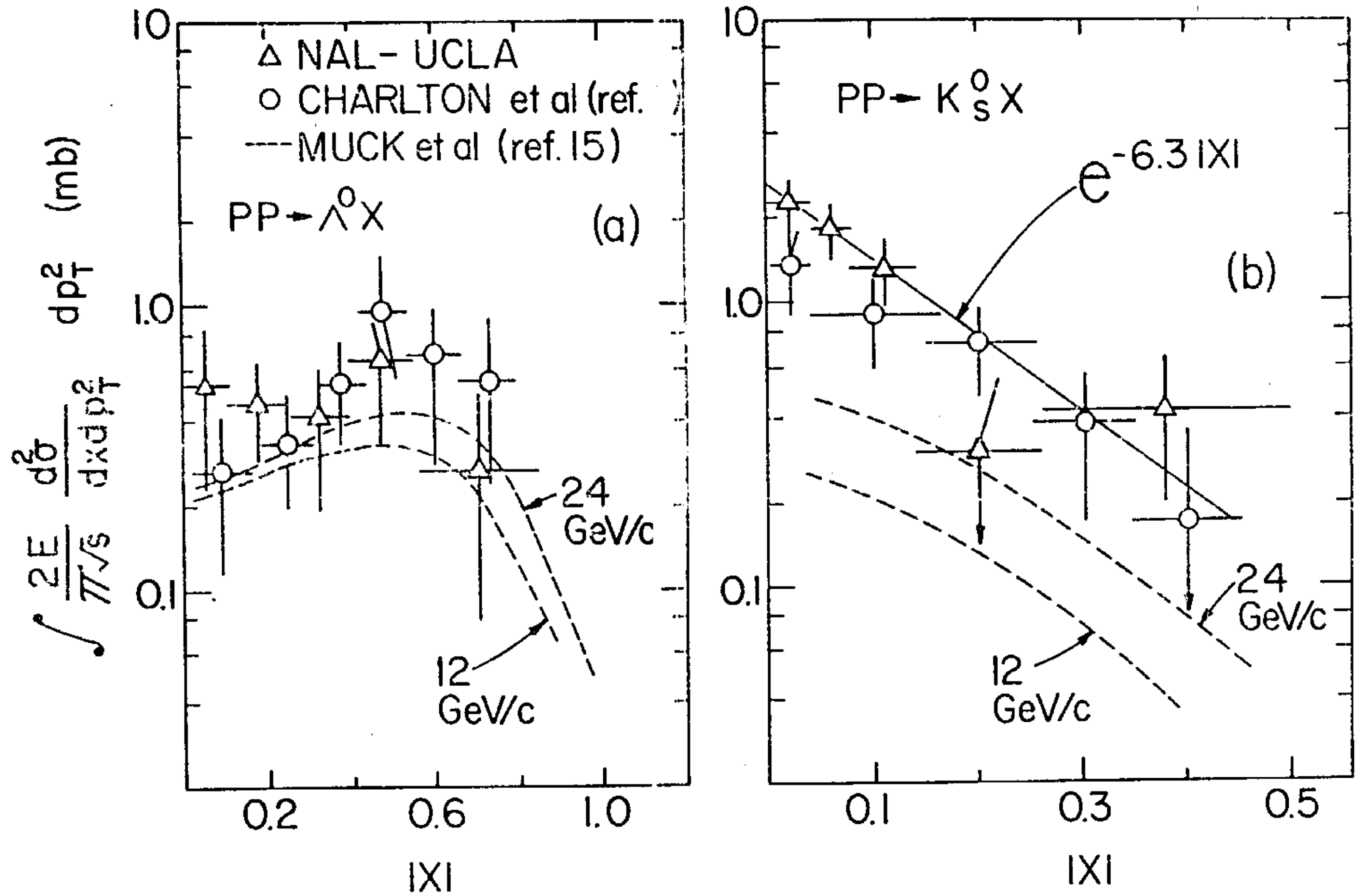


Fig. 7. The invariant cross section integrated over $P_t^2$ versus x for (a) $pp \rightarrow \Lambda^o X$ and (b) $pp \rightarrow K_s^o X$.

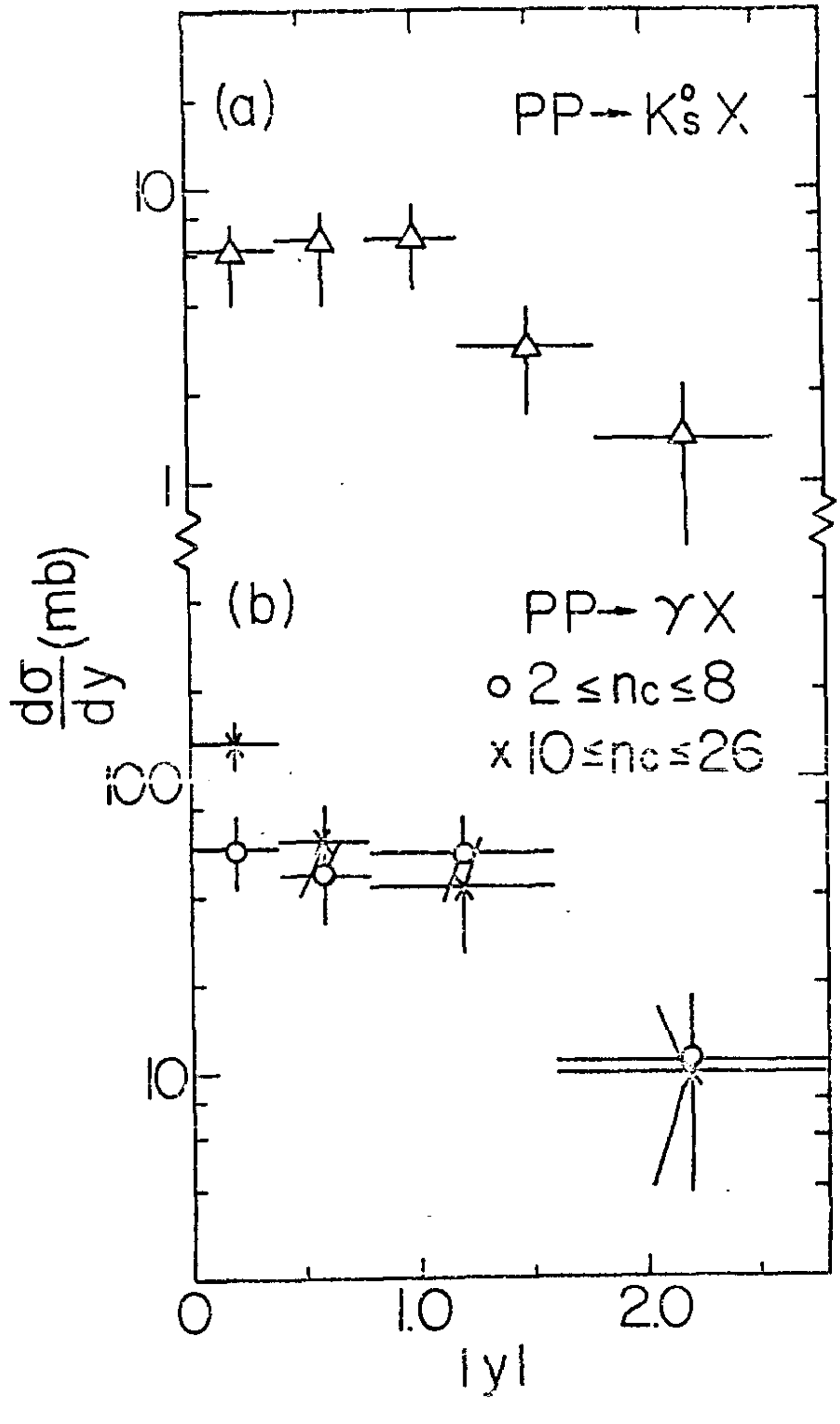


Fig. 8. dσ/dy versus y for (a) pp → $K_s^o$X and (b) pp → γX.

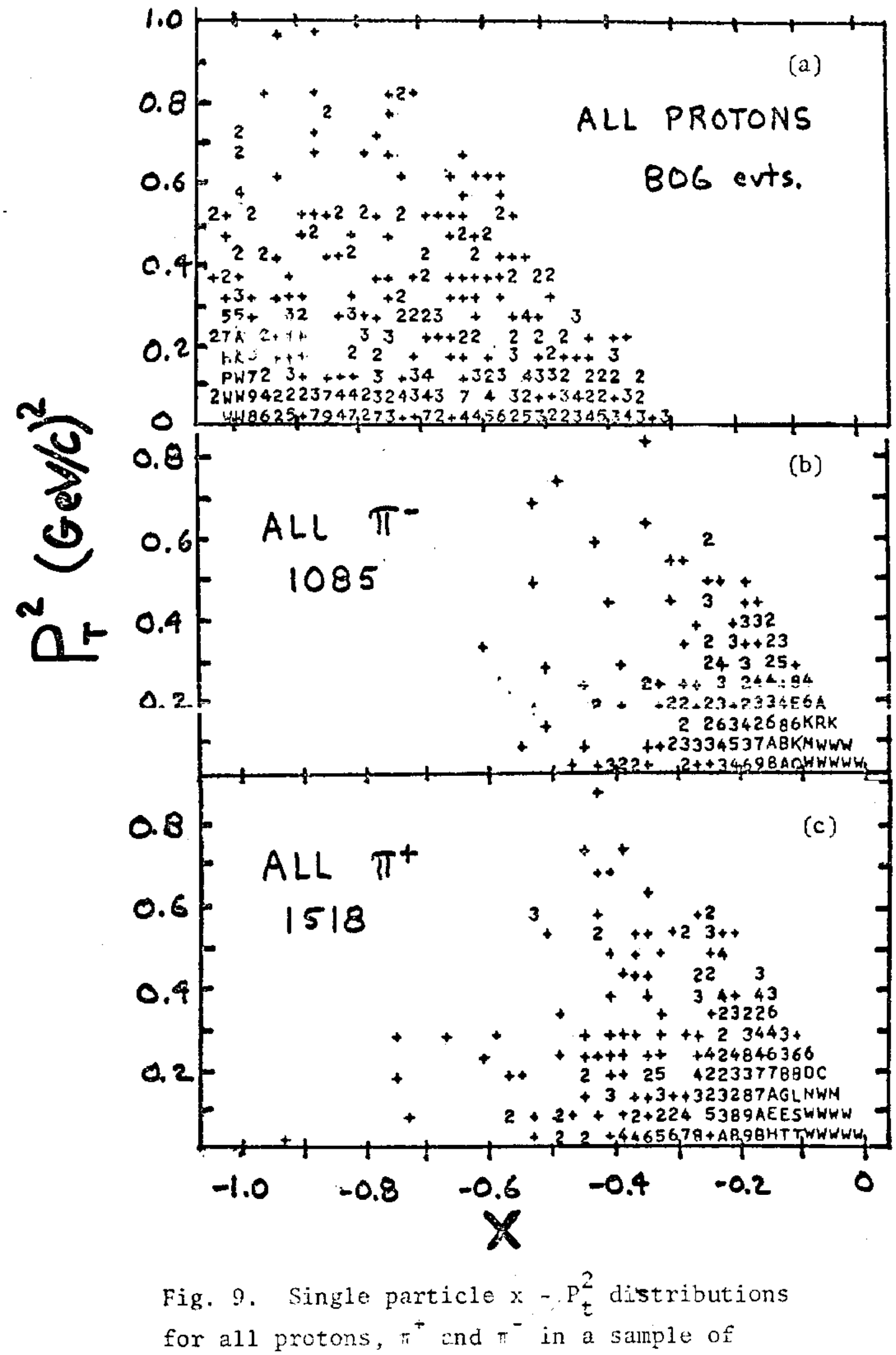


Fig. 9. Single particle x - $P_t^2$ distributions for all protons, $\pi^+$ and $\pi^-$ in a sample of 1750 events.

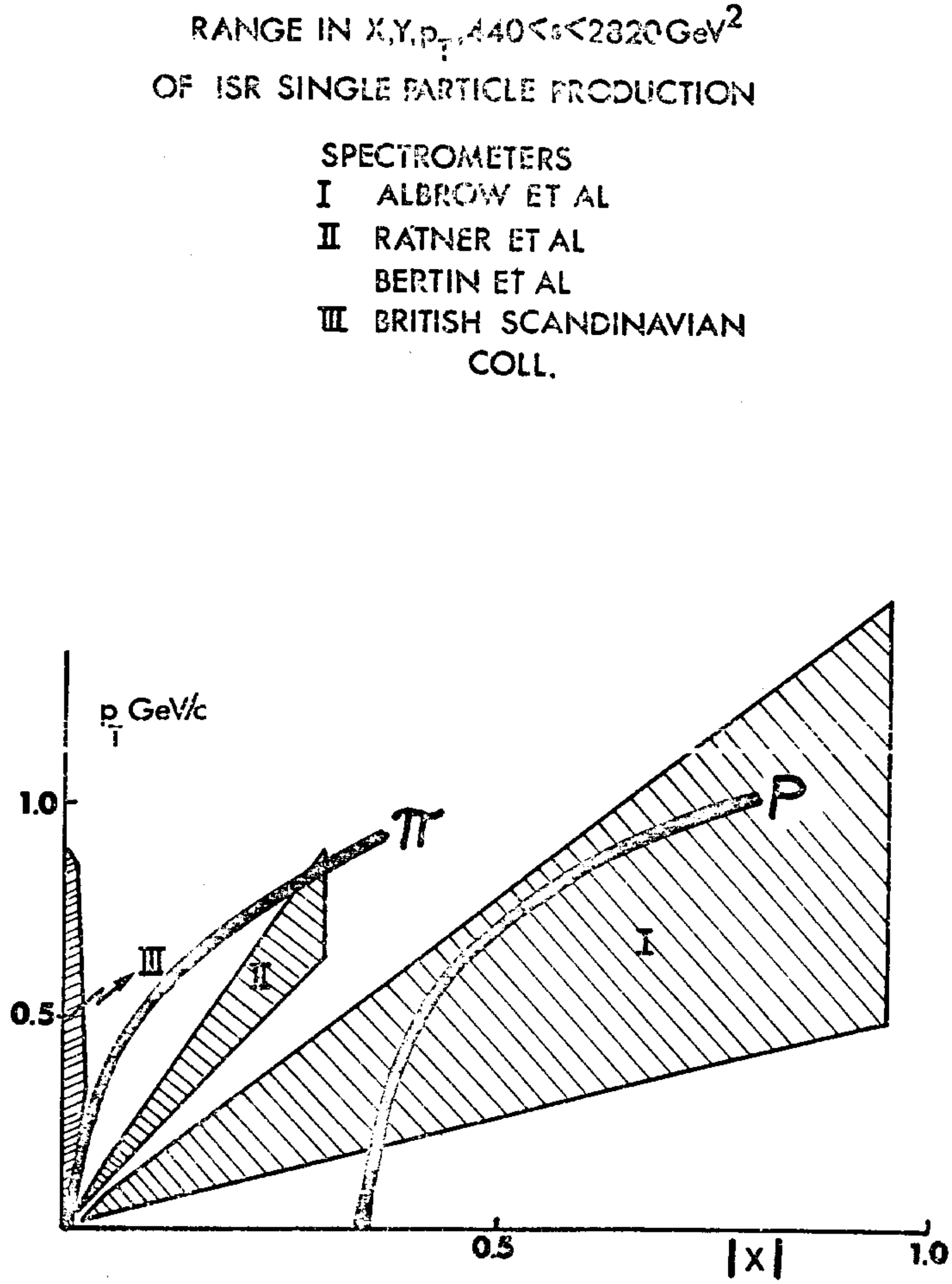


Fig. 10. $P_t$ - x regions for ISR and NAL slow pion and proton data.

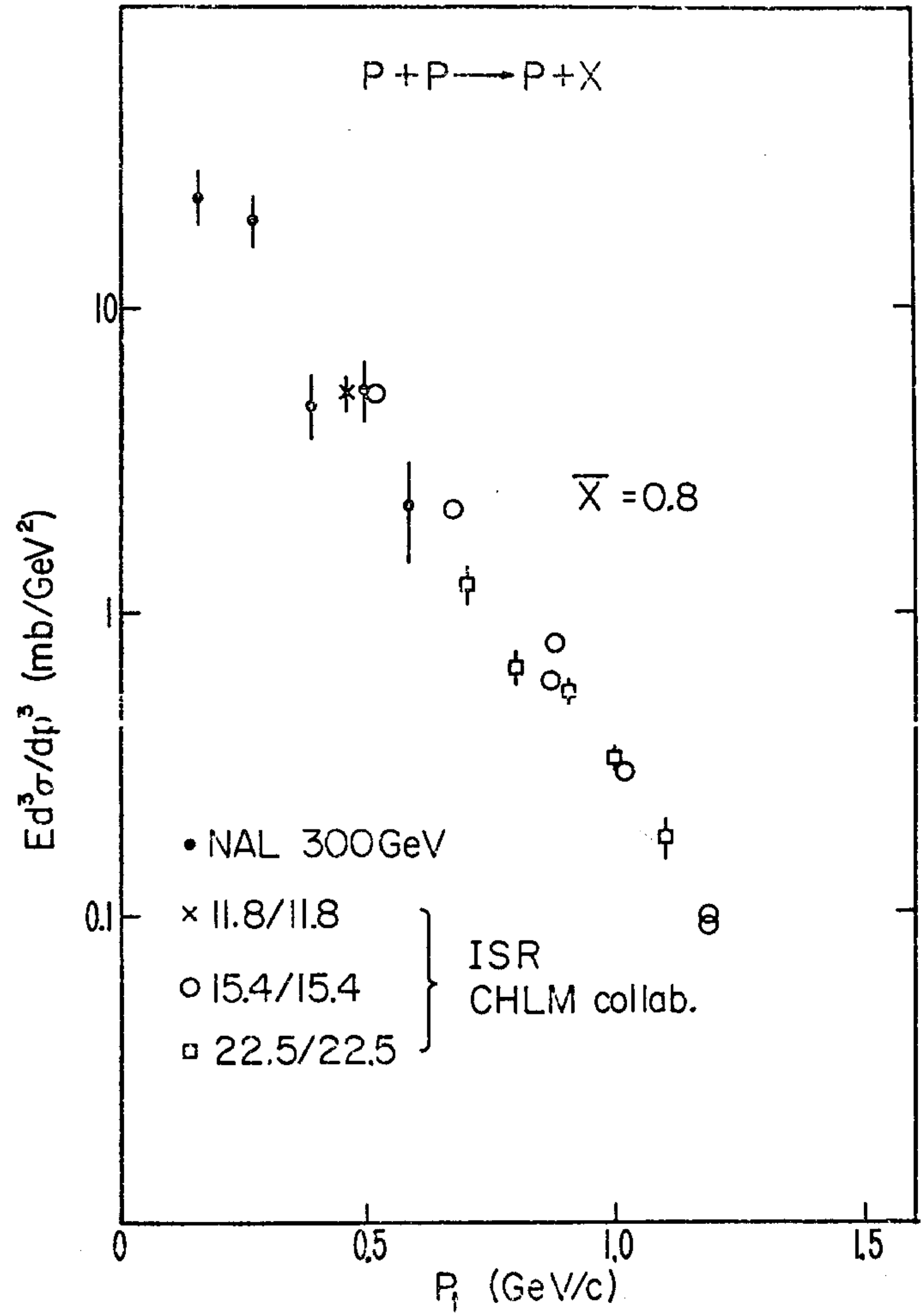


Fig. 11. $P_t$ distribution for protons at a mean $\overline{x}$ = 0.8 (0.7 to 0.9). Data is compared to that of the CERN-Holland-Lancaster-Manchester collaboration (Albrow et al.).

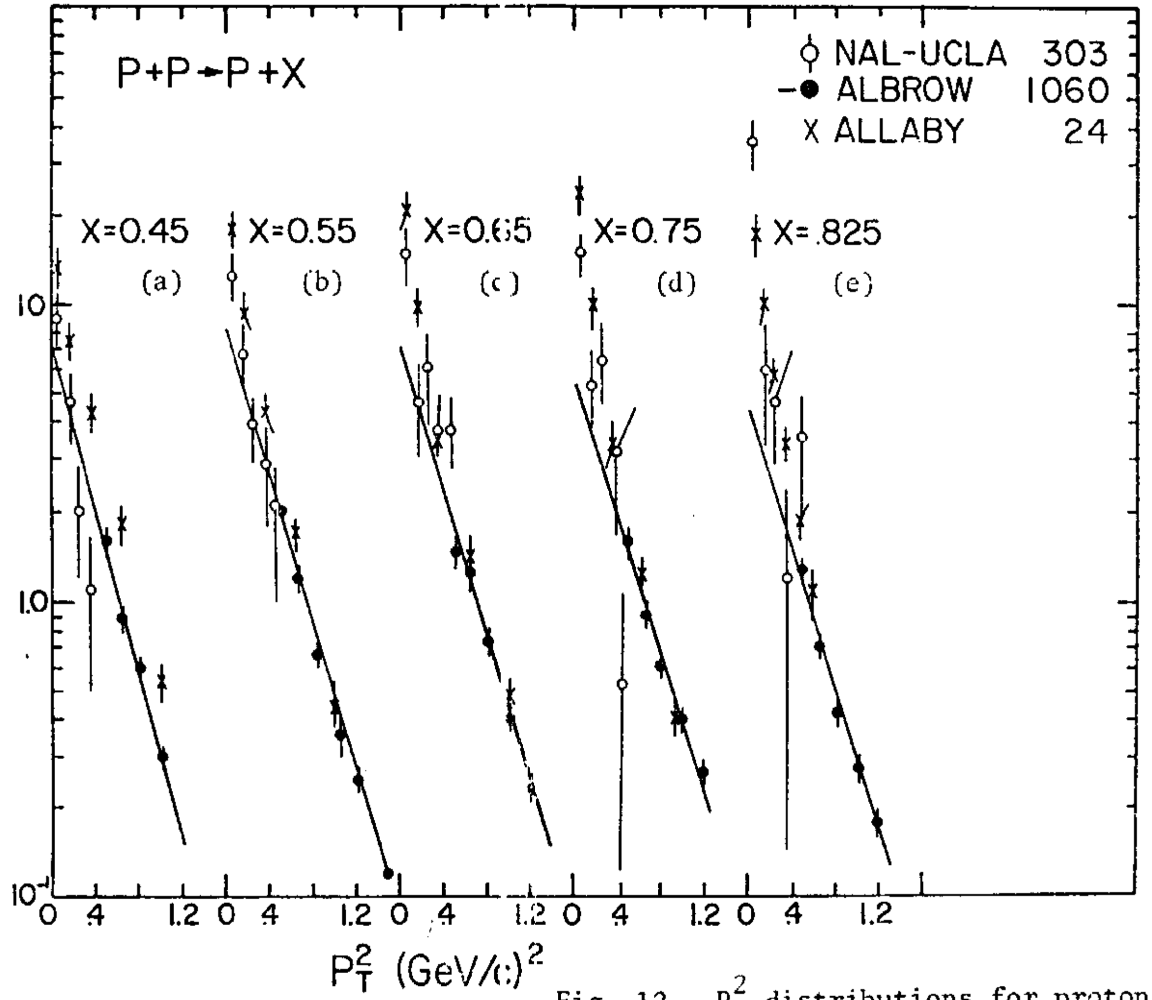


Fig. 12. $P_t^2$ distributions for protons at $\bar{x}$ = 0.45, 0.55, 0.65, 0.75, and 0.825. This data is compared with the ISR data of Albrow et al. and the 24 GeV/c data of Allaby et al.

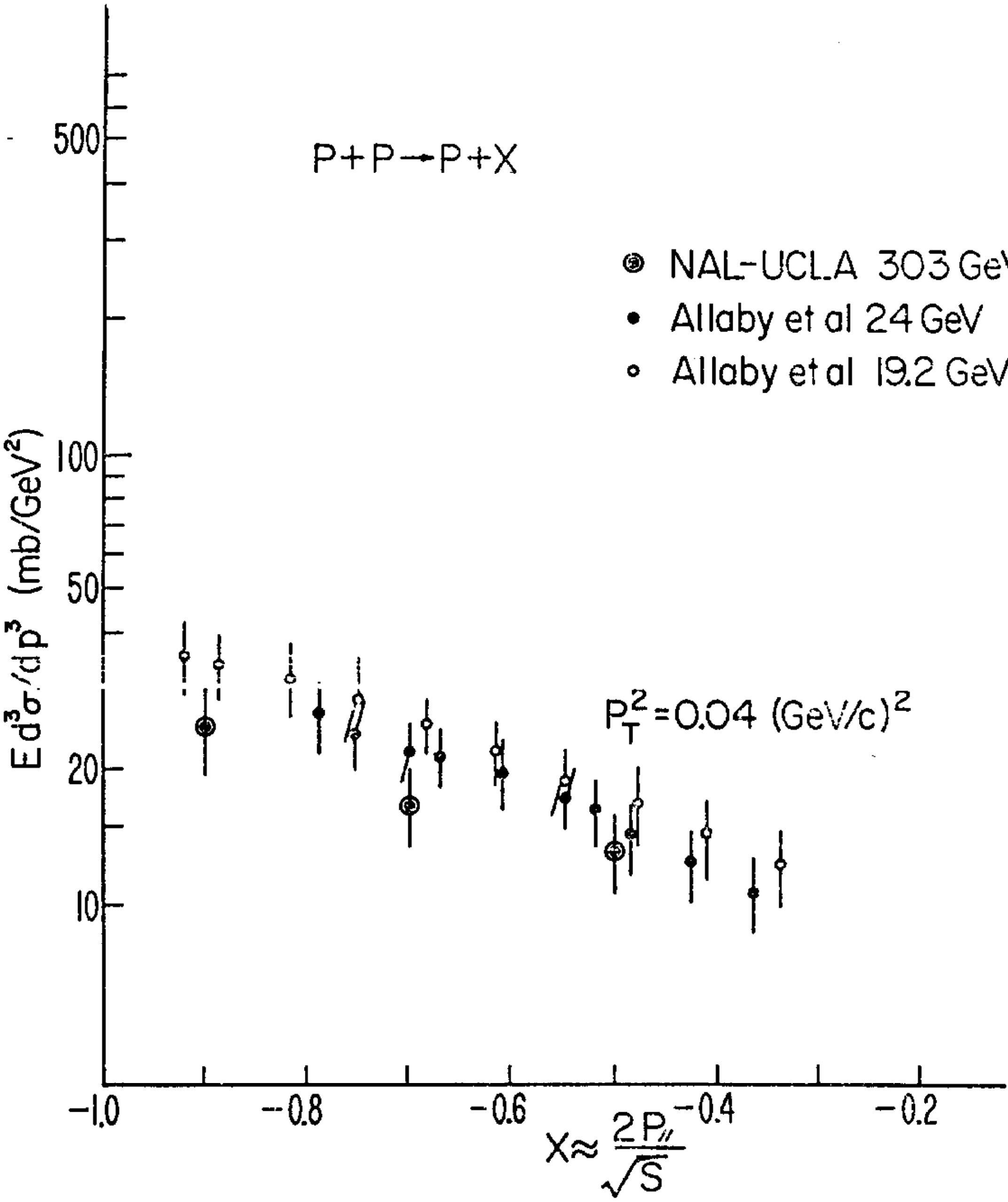


Fig. 13. x distribution for protons at $P_t^2$ = 0.04 (0.02-0.06) $(GeV/c)^2$.

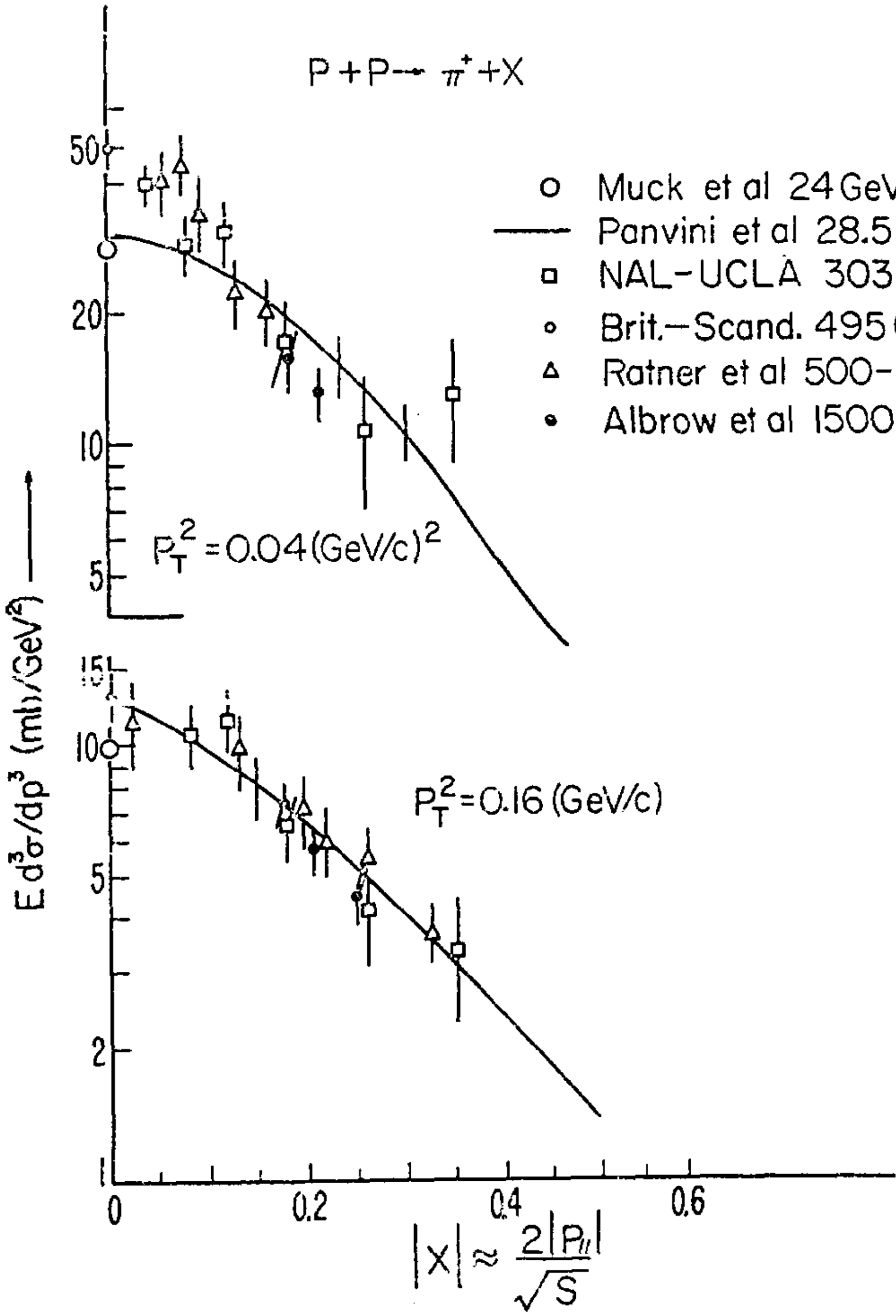


Fig. 14. $x$ distributions of $\pi^+$ at $P_t^2 = 0.04$ and 0.16 $(GeV/c)^2$. Comparison is made with the ISR data and the low energy data of Panvini et al. and Allaby et al.

NAL-Conf-73/31-EXP
7200.037

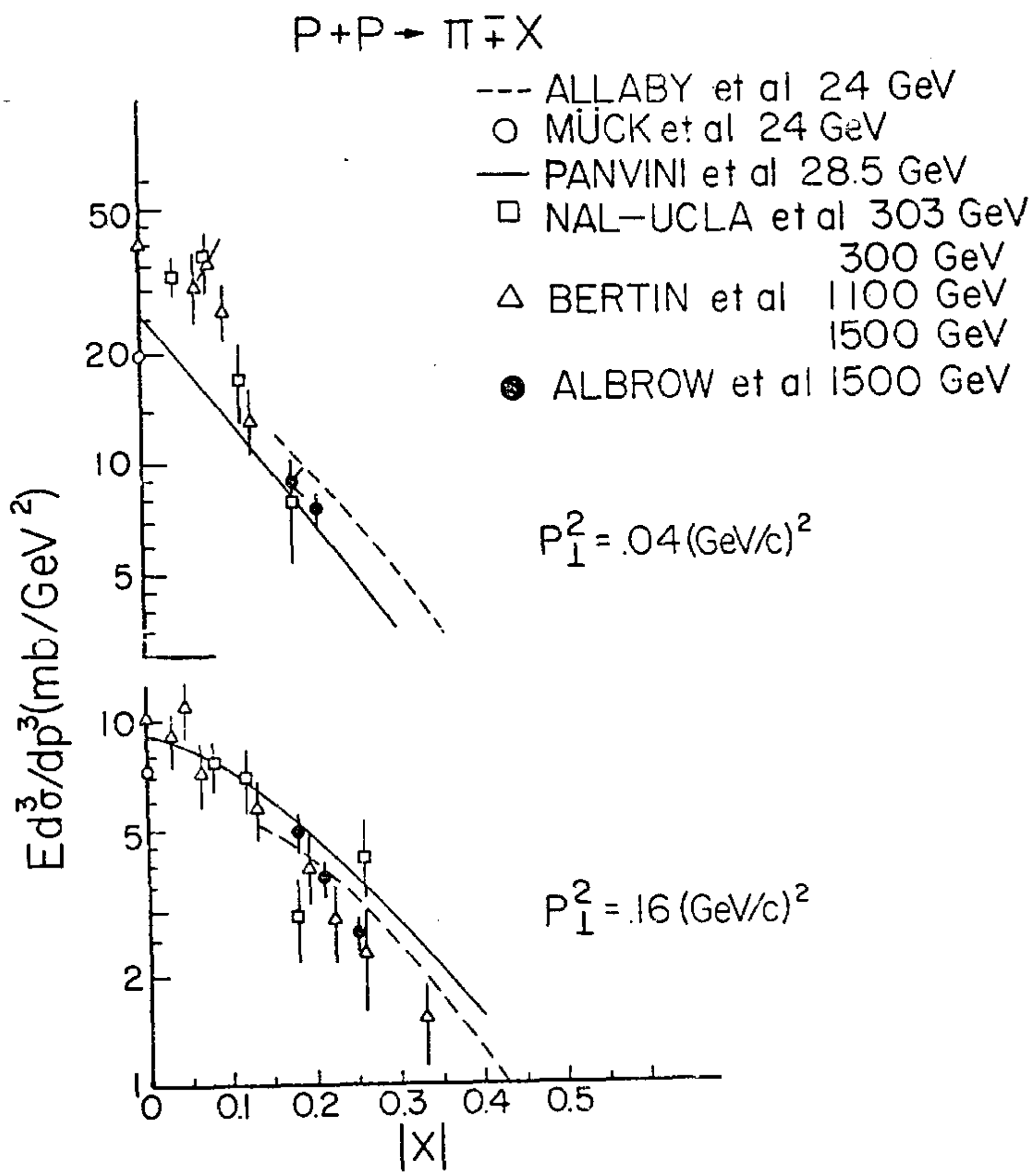


Fig. 15. x distributions of $\pi^-$ at $P_t^2$ = 0.04 and 0.16 $(GeV/c)^2$.

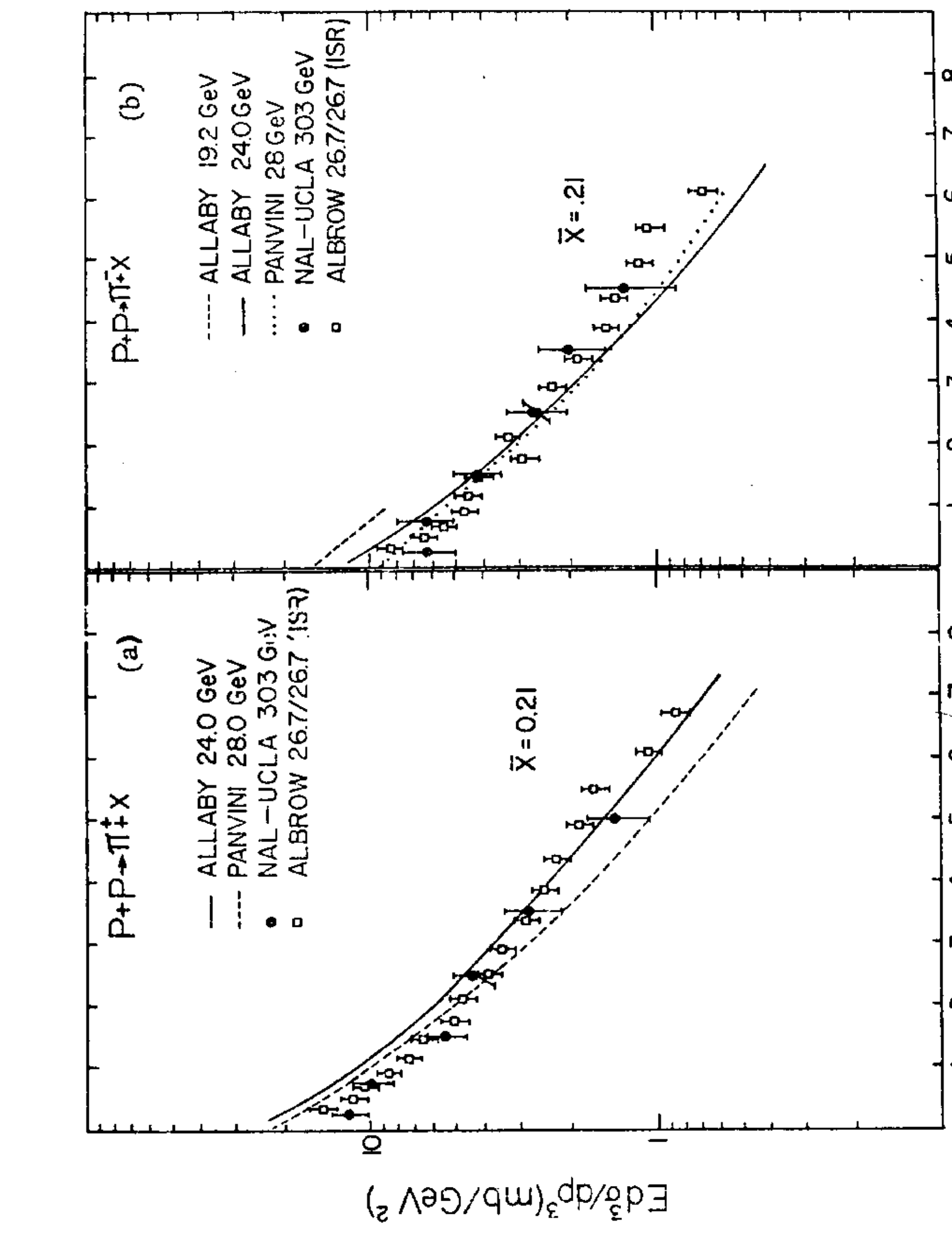


Fig. 16. $p_t^2$ distributions for $\pi^+$ and $\pi^-$ at $\bar{x} = 0.22$.